Self-Assembly for Two Types of J-Aggregates: Cis-Isomers of Dye on the Carbon Nanotube Surface and Free Aggregates of Dye Trans-Isomers

Petro Lutsyk[a,b,*], *Yuri Piryatinski*[b], *Mykola Shandura*[c], *Mohammed AlAraimi*[a,†], *Maria Tesa*[d], *Georgios E. Arnaoutakis*[d,e], *Ambrose Ashwin Melvin*[e], *Oleksiy Kachkovsky*[f], *Anatoly Verbitsky*[b], *Aleksey Rozhin*[a]

[a] Nanoscience Research Group & Aston Institute of Photonic Technologies, School of Engineering & Applied Science, Aston University, Aston Triangle, B4 7ET Birmingham, UK.

[b] Institute of Physics, National Academy of Sciences of Ukraine, 46, prospekt Nauky, 03680 Kyiv, Ukraine.

[c] Institute of Organic Chemistry, National Academy of Sciences of Ukraine, 5, Murmanska str., 02660 Kyiv, Ukraine

[d] Edinburgh Instruments Ltd, 2 Bain Square, Kirkton Campus, Livingston EH54 7DQ, UK.

[e] Department of Solar Energy and Environmental Physics, Jacob Blaustein Institutes for Desert Research, Ben-Gurion University of the Negev, Midreshet Ben-Gurion, 84990, Israel

[f] Institute of Bioorganic Chemistry and Petrochemistry, National Academy of Sciences of Ukraine, 1, Murmanska str., 02660 Kyiv, Ukraine.

* Corresponding author; email: p.lutsyk@aston.ac.uk

† Present address: Higher College of Technology, Al-Khuwair, PO Box 74, Postal Code 133, Sultanate of Oman.

ABSTRACT. Development of novel nanoscale devices requires unique functional nanomaterials. Furthermore, chemical design of different nanoparticles in one unit is a complex task, particularly the application of self-assembly J-aggregates, which can substantially advance the nanomaterial's properties due to resonant delocalization of excitons. Here, we have demonstrated for the first time formation of resonantly coherent J-aggregates on carbon nanotubes with highly efficient energy transfer from the aggregates to the nanotubes. All energy of photons absorbed by the aggregates is conveyed to the nanotubes, completely quenching the J-band emission and photosensitizing the nanotubes. Overall, we discovered formation of two types of J-aggregates, where one type is related to self-assembly of cis-isomers on the nanotube surface and second type is associated to self-organizing trans-isomers into free J-aggregates without the nanotubes. Importantly, the J-aggregates on carbon nanotubes with strong energy transfer peaks of photoluminescence in near infrared range is of high interest for practical applications on biomedical imaging, nanoscale optoelectronic and nanophotonic devices.

Introduction

Development of nanoscale functional devices has become a feasible objective for scientific and industrial community due to recent advancements in the field of nanomaterials chemistry and instrumentation.[1,2] Application of molecular self-assembly for functionalization and fabrication of nanosize structures leads to controlled and simple fabrication techniques enabling practical use of nanoscale innovations.[3,4] One of the most intriguing supramolecular self-assemblies are J-aggregates formed by strong non-covalent coupling of multiple molecules into prolonged 'staircase'-type stacking.[5] The coupling results in strong coherent resonance of delocalized excitons, and such excitons can easily migrate inside J-aggregates. Since their discovery, J-aggregates gained widespread interest and application as spectral sensitizers in film photography,[6] and now they have obtained a revival of scientific attention for advanced applications in nanoscale photonics and optoelectronics.[5-7] Due to their unique properties, J-aggregates have become promising in the areas of light emitting diodes (LEDs),[7,8] excitonic-plasmonic devices and optical microcavities,[9,10] quantum computing and optical switching,[6,8] transistors,[11] bio-medical imaging.[6,12,13] Thus, J-aggregates are extraordinary functional materials obtained via chemical engineering of supramolecular self-assembly.

Coherent coupling between J-aggregates and other nanomaterials provides opportunity to not only combine their best features, but to obtain novel advanced nanomaterials.[5-7] For example, Vasa et al. have observed ultrafast energy transfer in J-aggregate/metal nanostructures being of high interest for all-optical ultrafast plasmonic circuits and devices.[14] Furthermore, the interaction of J-aggregates with biological materials has strong practical focus in bioimaging[12] and theranostics.[13] There are plenty of other application-targeted J-aggregate interactions with DNA,[15] carbon nanotubes,[16-18] etc.[6,10] Recently, Gaufres et al. have revealed that some dyes can form weak J-

aggregates inside carbon nanotubes having a high potential in robust multispectral imaging via giant Raman scattering.[19] However to the best of our knowledge, there are no literature on formation of resonant J-aggregates on the outer surface of the nanotubes enabling to explore strong synergetic effect due to the interaction between them. The resonant narrowband redshift energy levels of the J-aggregate could align with the narrow exciton levels of the nanotubes and result in resonant exciton-coupled hybrids of J-aggregate-nanotube.

In this paper, we report on the discovery of highly resonant J-aggregates formed on the outer surface of single-walled carbon nanotubes (SWNTs) evidencing very efficient energy transfer from the aggregates to the nanotubes. We show for the first time that SWNTs are acting as both scaffolding frames for J-aggregation as well as efficient acceptors of the energy from the aggregates of benzo[e]indocarbocyanine (BIC) dye (Figure 1a). BIC is a shorter analogue of well-known "Indocyanine Green" dye employed into medical diagnostics,[20] which broadens the prospects of studied system to be involved in life sciences.

Experimental Section

(a) Materials. The BIC dye was synthesized in the Institute of Organic Chemistry (National Academy of Sciences of Ukraine). The dye purity of 98% was determined by liquid chromatography - mass spectrometry (LC-MS). The concentrations of aqueous solutions of BIC were studied in the range of (0.1-0.001)·g/L (molar concentrations are exemplified in Supporting Information). BIC molecule dissociates in the solution into the positively charged conjugated part with developed π-electron system and the negatively charged counter-ion - triethylammonium. The main spectral properties of the dye are determined by the conjugated part.

CG100 CoMoCAT SWNTs (purchased from SWeNT Inc.) were prepared in a similar manner as described in.[16] The purity of SWNT powder is defined by SWeNT Inc. as carbon content > 90 %, ≥70% ('carbon as SWNT'). The carbon nanotube powder (1.2 mg) was dispersed in deionized water (20 mL) in the presence of sodium dodecylbenzene sulfonate (SDBS) (6.5 mg). Bath ultrasonication was performed by a NanoRuptor (Diagenode) processor for 1 hour at 250 W and 21 kHz. The SWNT dispersions were centrifuged for 1 hour with an Optima Max-XP ultracentrifuge (Beckman Coulter) at 30 000 rpm (MLS 50 rotor) to remove the nanotube bundles and to get well purified supernatant dispersion of SWNT. We have used alternative surfactants[16] to disperse SWNTs, such as sodium dodecylsulfate (SDS; 6.5 mg), sodium deoxycholate (SDOC; 6.5 mg), sodium taurodeoxycholate (STDOC; 5.0 mg), polyoxyethylene octyl phenyl ether (Triton X-100; 15.2 mg), and polyvinylpyrrolidone (PVP; 19.2 mg). The SDBS purchased from Sigma Aldrich (289957) is technical grade material (approx. 90%) and may contain various isomers, however its infrared and NMR spectra conform to the SDBS structure. SDS (436143), SDOC (D6750), STDOC (T0875), Triton X-100 (X100) and PVP (PVP10) were purchased from Sigma Aldrich. NaCl was obtained from Acros Organics (424290250).

To prepare mixtures of BIC with SWNTs dispersed by SDBS, we used 10, 20, or 40% of the initial dispersions of SWNTs. From the estimate of SWNT concentrations made in our previous work,[16] the following concentrations of the nanotubes dispersed by SDBS were obtained depending on the dilution of the initial dispersions: 10% - 0.003 g/L, 20% - 0.006 g/L, and 40% - 0.012 g/L. The estimated mass concentrations of SWNTs will be used within the results and discussion for consistency. This way, the concentrations of SDBS in all samples of the three component mixtures (SWNT-SDBS-BIC) were in the range of (0.03-0.13) g/L. According to the literature, critical micelle concentration for SDBS is approximately 0.15 g/L,[21] thus the studied

mixtures have premicellar concentrations of SDBS. The concentration of SWNTs dispersed by SDS, SDOC, STDOC, Triton X-100 and PVP in the mixtures with BIC was 0.006 g/L.

(b) Experimental. The absorption spectra were measured with a Lambda 1050 UV/VIS/NIR spectrometer (Perkin Elmer). We used the 1 cm optical path quartz cells for all measurements except the solutions of BIC with concentration of 0.1 g/L were measured with TrayCells (Hellma) having an optical path of 1 mm.

The maps of PL excitation-emission, PLE maps, where the X axis is the wavelength of PL emission, λ_{EM}, and the Y axis is the wavelength of PL excitation, λ_{EX}, were measured by a NanoLog excitation–emission spectrofluorometer (Horiba Ltd). The spectrofluorometer is equipped with a silicon detector for visible range and a liquid nitrogen cooled InGaAs array detector for NIR range measurements. 2 and 10 nm entrance/exit slits were employed for the monochromators in visible and NIR ranges, respectively.

The time-resolved photoluminescence (TRPL) decays in visible range were measured with a LifeSpec II spectrofluorometer (Edinburgh Instruments Ltd) with excitation by a picosecond pulse diode laser at wavelength λ_{EX} = 405 nm and pulse duration 40 ps (EPL-405). The TRPL decay measurements in the NIR range were performed on an FLS980-D2D2 spectrometer (Edinburgh Instruments Ltd) with excitation by a Whitelase SCUV-3 supercontinuum laser (Fianium) via monochromator (λ_{EX} = 630 nm) operating at a repetition rate of 20 MHz. The bandwidth of the monochromator slits was set to 15 nm for the emission at 1038 and 1125 nm. Both TRPL spectrometers employ the time correlated single photon counting (TCSPC) technique and the decays were obtained in reverse mode. The lifetime data were obtained from exponential fitting of

PL decays using a F900 and a FAST software packages (Edinburgh Instruments Ltd) taking into account instrument response functions (IRF).

Transmission electron microscopy (TEM) images were obtained with a transmission electron microscope (Tecnai, T12 G^2 TWIN) operating at 120 kV. We used LC300Cu Lacey Carbon support films made of copper 300 mesh grids (EM Resolutions) for solid state samples of the studied systems. The statistics of the TEM images were processed by using ImageJ software analysis in the Region of Interest mode. After setting the intensity threshold to distinguish between sample and background, the area and mean intensity of high contrast pixels were calculated in the region of interest. The area calculated in % represents the surface coverage of TEM images by the samples, where 100% stands for images fully covered by the sample.

Results and Discussion

We have revealed resonant J-aggregates of BIC dye on the SWNTs of various chiralities dispersed with SDBS (Figure 1a-c). $S_0 \rightarrow S_1$ transition in J-aggregates (the right-hand side of Figure 1c) has lower energy than such transition in monomers (the left-hand side of Figure 1c) resulting in a new redshift peak.[4,5] The sharp redshift J-band appears due to the 'staircase'-type stacking of dye molecules enabling strong coherent resonance of delocalized excitons.[4-6] The aqueous solution of the dye having a pink color and the monomer absorption peak at 583 nm immediately change in the presence of SWNTs to a blue color featuring a new very sharp peak at 632 nm (Figure 1d). The degree of redshifting, defined as a difference between the absorption peaks of a monomer and J-aggregate (Figure 1d), is characterizing strength of interaction in such resonant stacking.[6] The reference samples containing two components only, dye and SDBS, do not result in such changes evidencing a key role of SWNTs in this process. The new narrow

absorption peak at 632 nm (curve 1 in Figure 1d) features J-aggregation of BIC molecules on the nanotubes. Formation of BIC's J-aggregates is unlikely for both the neat solutions of the dye at low concentrations (10^{-6}-10^{-4} M) and the SDBS-dye mixtures. Besides, testing the mixtures of SWNTs dispersed by various surfactants, such as SDS, bile salts, Triton X-100, etc., we could not obtain the J-aggregates as no sharp peak of J-band was observed for such systems (Figure 1e). Thus, the revealed process of J-aggregation is highly specific and working well for SDBS wrapped SWNTs as template-guided self-assembly. The uniqueness of J-aggregation aided by SDBS can be rationalized with the presence of the benzene ring in the molecular structure of SDBS. The aromatic hydrocarbon in SDBS is proven to facilitate highly efficient and stable SWNT dispersion,[17] and selective J-aggregation with SDBS could be related to specific π-stacking interaction of the SDBS aromatic ring with SWNTs. Recently, we reported on the J-like aggregation of cyanine dyes on carbon nanotubes, but the sharp redshift peak of resonant J-aggregates was never achieved before.[16-18] The broad peak of J-aggregation evidences a lack of strong coupling for supramolecular delocalization of coherent excitons.[16,18] Therefore, previously reported dye-SWNT systems cannot fully benefit from extraordinary J-aggregate properties in terms of ultra-fast and high-resonance interactions, which can be achieved for BIC J-aggregates on SWNTs.

A ratio of concentrations for the aggregated dye and SWNTs allows us to characterize the coverage of the nanotubes by J-aggregates. The straightforward way to evaluate the coverage is to determine the samples where all the dye molecules in the mixture form J-aggregates. A lack of monomer signature in the spectra of the mixtures evidences that practically all the dye molecules are aggregated. We have it only at the 0.012 g/L concentration of the nanotubes and the dye concentration of 0.004 g/L resulting in the coverage ratio of 1/3 $g_{(BIC)}/g_{(SWNT)}$.

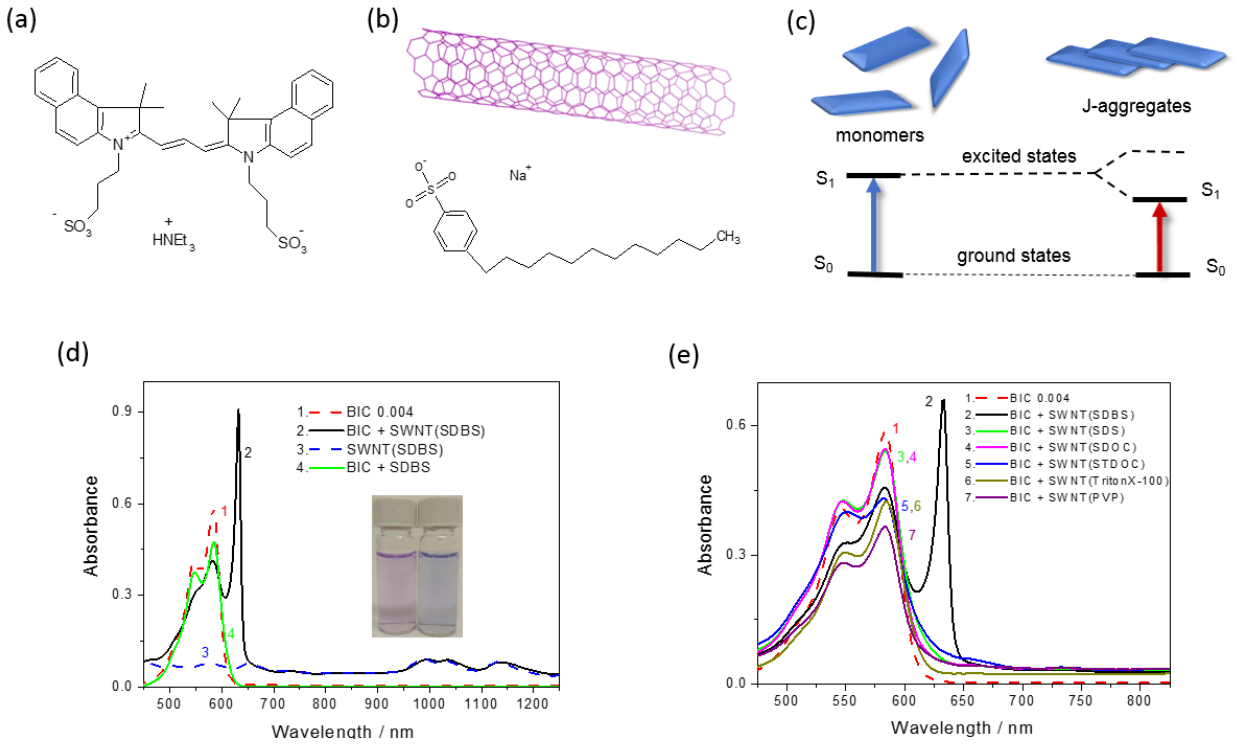

Figure 1. (a,b) Molecular structure of BIC dye (a), SWNT and SDBS (b). (c) Schematic diagram of absorption energy levels for dye monomers (left) and J-aggregates (right). (d,e) Absorption spectra for solution of BIC (curves 1 in d,e), mixtures of BIC with SWNT dispersed by SDBS (curves 2 in d,e), dispersion of SWNT with SDBS (curve 3 in d), mixture of BIC with SDBS (curve 4 in d), and mixtures of BIC with SWNT dispersed by SDS (curve 3 in e), SDOC (curve 4 in e), STDOC (curve 5 in e), Triton X-100 (curve 6 in e), PVP (curve 7 in e). BIC concentration is 0.004 g/L, SWNT concentrations are 0.012 g/L (curves 2,3 in d) and 0.006 g/L (curves 2-7 in e); SDBS concentrations are 0.13 (curves 2,3 in d) and 0.05 g/L (curve 4 in d); (d) Inset depicts vials with the BIC solution (left) and the mixture of BIC with SWNT (right).

We have also studied BIC aggregation without the nanotubes aiming to understand the aggregation process of the dye on SWNTs. The BIC molecules aggregate at the high

concentrations in the range of 0.1 g/L (Figure 2a-c) and at lower concentrations (0.004 g/L) in the presence of inorganic salt - NaCl (Figure S1). We name the J-aggregates of BIC formed without SWNTs as "free J-aggregates", and the reason for this is that there are some characteristic features of such system. The narrow redshift absorption peak of free J aggregates has a maximum at 640 nm being more redshifted than the 632 nm peak of the SWNT system (Figure 2a, curves 2,3; Figure S1a). Another distinguishing feature of the free J-aggregates is their strong photoluminescent (PL) emission in the visible range. The maps of PL excitation-emission, PLE maps, where the X axis is the wavelength of PL emission, λ_{EM}, and the Y axis is the wavelength of PL excitation, λ_{EX}, are excellent tools to characterize the emission of the monomers, SWNTs, J-aggregates, etc. (Figure 2-3). Free J-aggregates have a narrow PL maximum at λ_{EX} = 640 nm and λ_{EM} = 640-645 nm (Figure 2ab, Figure S1), which is fully quenched in J-aggregates on SWNTs (Figure 2e). The quenching is well discriminated via comparison of the PLE maps (Figure 2b,e) in the area of λ_{EX} = 610-630 nm and λ_{EM} = 640-645 nm. Additionally, two PL peaks at the cross-section of λ_{EM} = 640 nm with λ_{EX} = 560 and 540 nm (Figure 2e) belong to the vibrational transitions in the BIC monomers. Thus, there is no visible range emission of J-aggregates on the SWNT. Furthermore, the free J-aggregates, formed at high concentrations of BIC or in the presence of inorganic salt shifting ionic balance of the aggregation process, have well distinguished nature in comparison with the SWNT based J-aggregates. Therefore, the curved carbon nanotube surface is a good nucleation frame to distinct J-aggregation of BIC molecules.

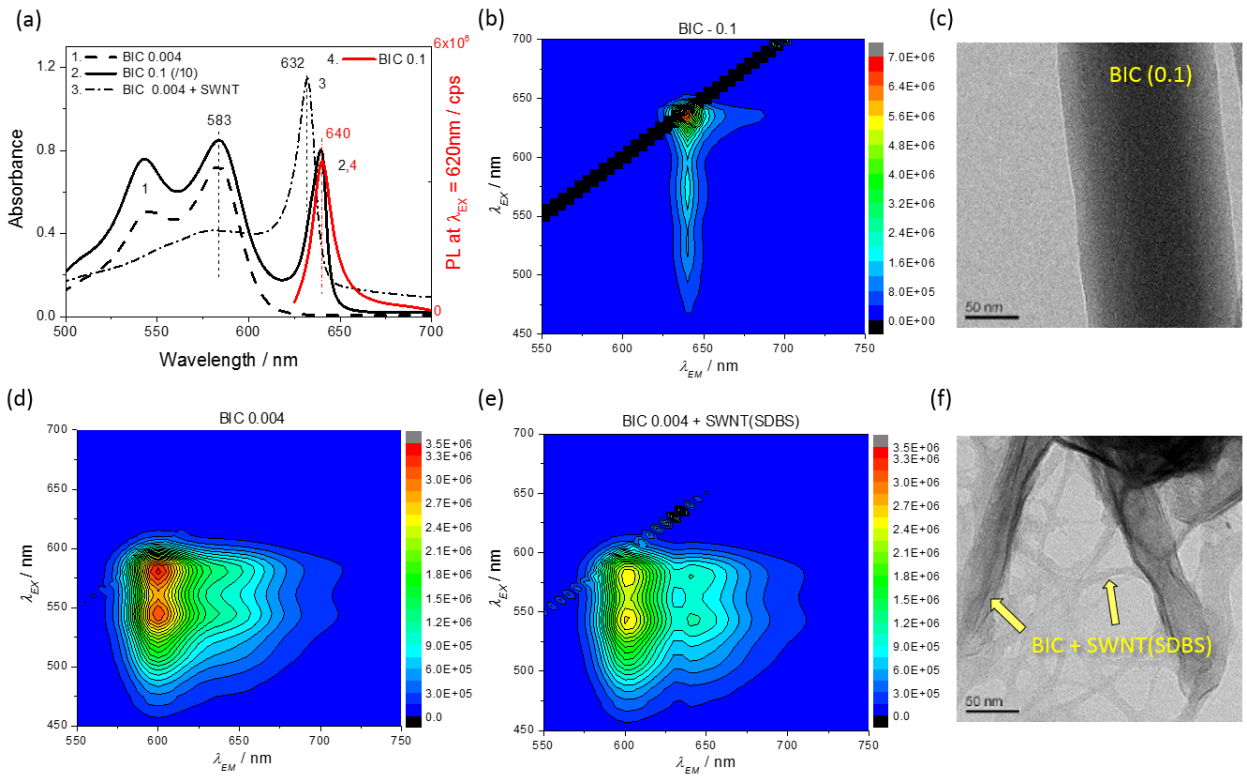

Figure 2. (a) Absorption spectra for solutions of BIC at 0.004 (1) and 0.1 g/L (2; magnitude divided by 10 to fit the graph scale), and for mixtures of BIC with SWNT (3); PL spectrum for solution of BIC at 0.1 g/L (4). (b,d,e) PLE maps for solutions of BIC at concentration of 0.1 (b) and 0.004 g/L (d), and for mixture of BIC at concentration of 0.004 g/L with SWNT (e). SWNT and SDBS concentrations are 0.012 and 0.13 g/L, respectively (a,e). (c,f) TEM images for BIC at concentration of 0.1 g/L (c) and mixture of BIC at concentration of 0.004 g/L with SWNT (f).

J-aggregates formed on SWNT transfer all energy of the excited states to the nanotubes and become completely quenched, whereas free aggregates have bright emission with small Stokes shift from narrow absorption peak (640 nm). To evidence the J-aggregate formation on SWNTs we studied TEM images for solid states of the dye-SWNT system and the neat dye at high

concentration. TEM images of the free aggregates have a prolonged rectangular form (Figure 2c; Figure S2), and the BIC-SWNT aggregation is evidenced as stripes of the dye aggregate framed by several SWNTs (Figure 2f) and extensive networks of the dye covering the nanotubes (Figure S3 and S4). The neat BIC molecules tend to form long and straight aggregates, and in the presence of SWNTs the BIC aggregation is facilitated by the elongated nanotubes working as scaffolding frames. Comparison of TEM images for studied SWNTs without and with the dye provides an apparent evidence that the SWNTs without BIC are bundling into clusters of a limited space (Figure S3), whereas the aggregation of the dye on the nanotubes helps to expand the network to web-like patterns of several micrometers (Figure S4). In addition, the statistical analysis of such networks via setting threshold of high contrast mode (Figure 2cf, Figure S3 and S4) shows that the area and mean intensity of high contrast pixels are larger in most of the SWNT-BIC samples than the same parameters in the neat SWNT. For example, the SWNT-BIC samples are covering area in the range of 33-64% and neat SWNT has 24-30% coverage; averaged by size of studied TEM images, we obtained the average area of the SWNT-BIC networks of 38% and the neat SWNT clusters of 28%. Thus, we evidence that dye molecules aggregate around the nanotubes covering SWNTs and form extensive SWNT-dye networks in solid state.

The essential feature of BIC-SWNT aggregates is highly efficient resonant energy transfer (RET) from the J-aggregates to SWNTs (Figure 3). This is evidenced by both completely quenched aggregate emission in visible range and an emergence of new excitonic peaks of PL (E^J_{11}) from near infrared (NIR) levels of SWNTs at the resonant excitation wavelength (λ_{EX}) 630 nm. The PLE map of neat CoMoCAT SWNTs with predominant (6,5), (7,5), & (8,4) chiralities have intrinsic PL peaks at E_{22} λ_{EX} = 570, 650, & 590 nm, respectively, and pertinent E_{11} λ_{EM} in the range of 950-1150 nm (Figure 3a). The RET from BIC aggregates results in an emergence of strong PL peaks

(E^J_{11}) at λ_{EX} = 630 nm matching the sharp absorption maximum at 632 nm. Furthermore, in the presence of BIC, the E_{11} nanotube intrinsic emission peaks are moderately (30-50%) quenched. The quenching of nanotube intrinsic emission is evidencing a close distance between the dye and nanotubes enabling its strong interaction and affecting PL peaks of the nanotubes.[18,24] It should be noted that E^J_{11} are slightly (3-10 nm) redshifted regarding to E_{11} of the pristine SWNT (Figure 3; Figure 4a). Analysis of literature shows that a complete quenching of PL due to the RET is happening at a close distance between a donor and an acceptor.[18,22] In the case of surfactant molecules restricting a close approach between the dye and SWNT, there is a partially quenched emission from the aggregated molecules.[16] Thus, we evidence a close distance of BIC J-aggregates to the SWNT surface enabling efficient RET due to a strong non-covalent donor-acceptor (D-A) interaction of the J-aggregates and SWNTs covered by SDBS.

On the right-hand side of Figure 3, the schematic diagrams of energy pathways in the studied systems is drawn. The energy structure of the SWNTs changes via formation of new local levels, $E^J_{11,}$ and potentially E^J_{22}, due to the D-A interaction between the nanotube and the J-aggregate. E^J_{22} should be located slightly below E^J level, so in the energy diagram these two levels are shown as overlapping into a single one (Figure 3b). The J-aggregate on the SWNT acts as an antenna, which effectively absorbs energy of light and converts into the energy of a migrating exciton. The excitons in such J-aggregates are effectively trapped on local levels of the D-A complexes of the J-aggregates on SWNTs ($E^J_{22,}$ E^J_{11}) resulting in the emergence of strong PL peaks at λ_{EX} = 630 nm. In such D-A complexes, the mixed exciton states are possible combining excitonic properties of J-aggregates and SWNTs.[25] Such mixed exciton states have a high transition oscillator strength inherited from the Frenkel excitons in the J-aggregate, and this can be attributed to a significant increase in the quantum yield of PL from the E^J_{11} states.

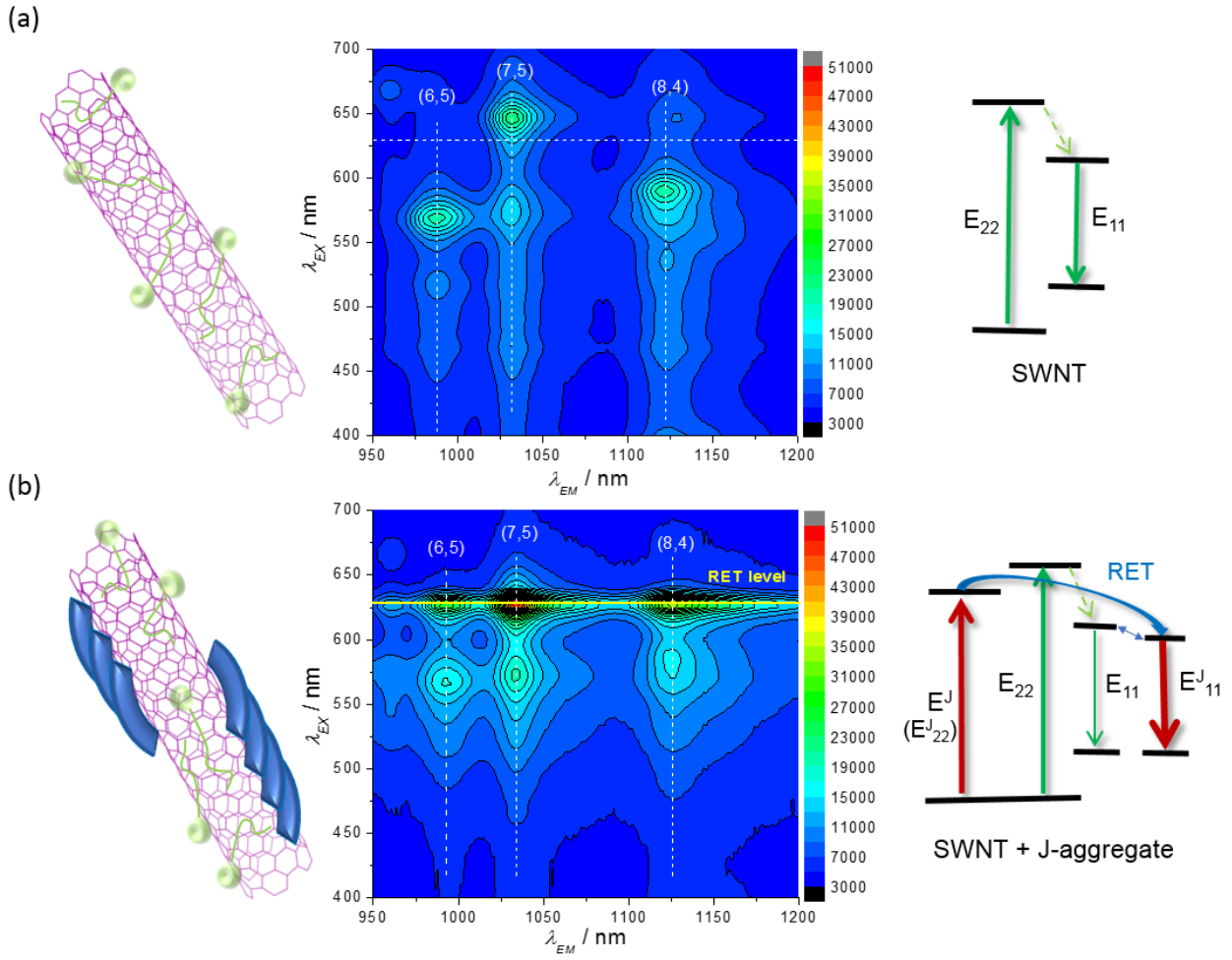

Figure 3. PLE maps for dispersion of SWNT wrapped with SDBS (a) and for mixture of BIC at concentration of 0.004 g/L with SWNT dispersed by SDBS (b). SWNT and SDBS concentrations are 0.012 and 0.13 g/L, respectively. Left-hand and right-hand side insets depict the supramolecular structure and the schematic diagrams of energy pathways in studied systems, respectively.

The RET from BIC aggregates to SWNTs of (7,5) chirality is energetically advantageous via E_{22}, whereas the RET to SWNTs of (6,5) and (8,4) chiralities should occur from the energy levels

lower than E_{22} energy levels of the pristine nanotubes, indicated by the absence of excitation peaks at $\lambda_{EX} > 630$ nm. The RET via the highest excited states from E^J (E^J_{22}) to E_{22} levels of the nanotubes is unlikely due to the high rate of vibrational relaxation. Therefore, the mechanism of direct RET from the E^J (E^J_{22}) to E^J_{11} levels omitting the E_{22} (Figure 3b) is favorable for all chiralities, even considering the very small spectral overlap integral between emission of the dye and E^J_{11} absorption of the nanotubes.[23] It should be mentioned that because of a small difference between the E^J_{11} and E_{11} levels [$(E_{11} - E^J_{11}) < kT$], the excitons can transfer from the local E^J_{11} levels to the E_{11} states via activation mechanism resulting in radiative recombination from these states. The direct RET from organic molecules to E_{11} emission levels of SWNTs might be also involved in other systems with excitation energy higher than E_{22}.[16,22,24] However the Dexter type RET to forbidden states of the acceptor (SWNT) is another alternative option,[26] which is hard to implicate, but should be taken into account. Besides, the large RET gap between the donor and acceptor levels should be treated as the gap for pristine nanotubes between E_{22} and E_{11} (Figure 3a).

An interesting feature of the BIC J-aggregates on SWNTs is a substantial growth of the RET peaks of PL due to the prolonged storage of the mixture (Figure 4a), whereas the absorption spectra alter very little with time (Figure 4b). In Figure 4a, displaying temporal change of PL spectra at $\lambda_{EX} = 630$ nm for the mixture of BIC with SWNT, we see approx. doubled PL intensity for SWNTs of (7,5) & (8,4) chiralities in 3 days; and the intensity of PL for SWNTs of (6,5) chirality has slowly grown from level of dark count noise to the level of PL for the (8,4) chiralities in 90 days. Essentially, there is no change in the bandwidth of absorption peak for J-aggregate (Figure 4b) showing no (or very slight) rearrangement of the molecules in the aggregates towards better ordering. It evidences that J-aggregates on SWNTs are formed during short time after the mixing, but the RET is not so efficient at the early stage of the aggregation. The RET is very sensitive to

the distance between the donor and acceptor,[23,26] and one of the reasons for the strong temporal PL sensitization could be the presence of a separation layer formed by SDBS between the aggregate and the SWNTs. Over time, the aggregates attracted by π-stacking interaction with SWNTs penetrate deeper into the surfactant shell becoming closer to the nanotubes. The effect is highly prominent for small diameter nanotubes, such as (6,5) chirality, which can form aggregates at a distance that prevent efficient RET due to geometry constraints, and only with time this distance becomes smaller enhancing RET. Another explanation of the RET PL increase is a change of mutual orientation of transition moments of the donors and acceptors, but it seems less likely because such behavior would be observed for all chiralities evenly.

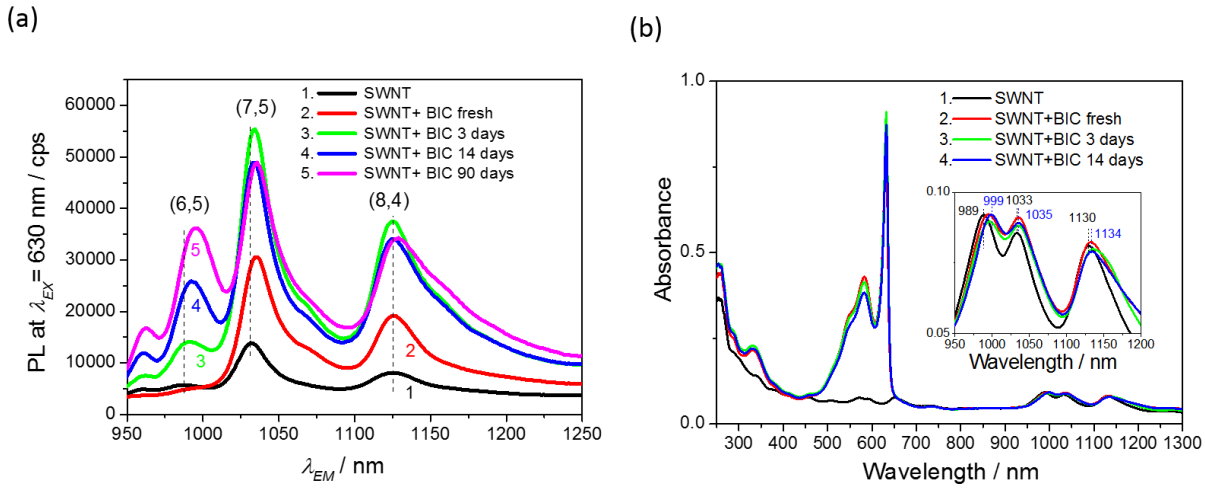

Figure 4. (a) PL spectra at λ_{EX} = 630 nm and (b) absorption spectra for SWNT dispersed by SDBS (1) and BIC mixtures with SWNT dispersed by SDBS (a: curves 2-5; b: curves 2-4). Time after the mixing is mentioned on the legends. The concentration of BIC, SWNT and SDBS concentrations are 0.004, 0.012 and 0.13 g/L, respectively.

Observed RET is associated with a strong quenching of PL for the J-aggregate donor. From PL data in Figure 2, we estimated the efficiency of RET in terms of donor quenching. In our estimation we considered that the PL emission of the J-aggregates on SWNTs without RET is same order of magnitude as the PL of free aggregate (approx. 10^6 cps). Assuming that the quenching is mainly due to the RET from J-aggregate to SWNT, the efficiency of RET (η) is defined from a ratio of SWNT aggregate PL (below noise level of 10^3 cps - Figure 2e) to free aggregate PL (10^6 cps - Figure 2b): $\eta = 1 - 10^3/10^6 \geq 0.99$.[22,23] High value of η shows that J-aggregate donor very efficiently transfer energy to the nanotube acceptor, however it does not consider the energy dissipation afterwards.

The excitation energy absorbed by the aggregates is non-radiatively transferred to the nanotubes, which emit this energy with much higher efficiency than that of intrinsic SWNT PL. The PL intensity at λ_{EX} = 630 nm for J-aggregates on SWNTs of (7,5) chirality increases about 3.8 times as it overlaps with the peak of neat SWNTs with maximum at λ_{EX} = 650 nm (Figure 3). The PL enhances 4.2 and 4.5 times for (8,4) and (6,5) chirality, respectively (Figure 3). Considering subtraction of instrumental dark count from the signal, the PL growth of more than one order of magnitude could be achieved for SWNT chiralities that do not emit light in the range of the RET, such as SWNTs of (6,5) chirality (Figure 3a). In general, it provides efficient sensitization of the nanotube emission at resonant λ_{EX}, however the quantum yield of such emission is restricted by a low quantum yield of the nanotubes and non-radiative relaxation in the RET process.[2] Sensitization of the SWNT emission in NIR range has a high potential for hyperspectral imaging of biological tissues[27] as well as for detection of the nanotubes in ambient environment.[16,18] In favor of this application, we evidence that the RET PL peaks grow with the increase of SWNT (Figure S5 and S6) and BIC concentrations (Figure S7). It should be noted that the growth of the RET PL peaks

with increased concentrations (Figures S5-S7) is highly dependent on SWNT's chirality with initial sensitization for the nanotubes of larger diameter. Furthermore, the mixtures at higher concentration of the dye (Figure S7) show that the number of BIC molecules physiosorbed to the nanotubes is limited (Table S1). The higher concentration of BIC molecules in the mixture results in increased monomeric contribution of the dye and practically constant extinction coefficient of the J-aggregate absorption at $(150 \pm 25) \cdot 10^3$ M^{-1} cm^{-1} (Table S1). In addition to imaging, such results could be also of high interest for biomimetic artificial light-harvesting[28] and imaging guided therapy,[13] as BIC analogues, such as "Indocyanine Green", are well-known in medical diagnostics.[20]

According to the literature, thiatrimethine analogues of BIC molecules also form J-aggregates.[29,30] Importantly, two possible types of J-aggregates were reported depending on the cis- and trans- isomerization of such dye molecules. Transition between cis- and trans-isomers of polymethine dyes substantially depends on the molecular structure of the dye and its environment,[30] like temperature, solvent rigidity, polarity, etc. Importantly, the J-aggregates of cis- and trans- form are distinguished by short and long wavelength J-aggregate peaks in their absorption and PL spectra. In our study, we also observe short (632 nm) and long (640-642 nm) wavelength peaks of SWNT based J-aggregates and free J-aggregates, respectively. Thus, we are able to assign the SWNT based J-aggregates to the cis form, and the free J-aggregates to the self-assembled trans-isomers of the dye. The reason for cis-J-aggregation favoring SWNT presence is that such process might require convex nano-tubular surface, which is preferable due to the bent geometry of the π-conjugated part of the stable cis-isomer.[29] Thus, we can be dealing with two different types of J-aggregates formed from cis-isomers on SWNTs and trans-isomers self-organizing into free J-aggregates. Reflecting on this outcome in general, J-aggregates of specific

cis-isomers can be designed due to presence nanotubular surfaces, and the properties of such J-aggregates will depend on the nanotube diameter, chirality, etc.

The measurements of time-resolved photoluminescence (TRPL) decays allowed us to determine the exciton lifetimes for studied aggregates. The lifetime determined from TRPL of the RET peaks in NIR (λ_{EM} at E^{J}_{11}) at the excitation λ_{EX} = 630 nm represents a hybrid lifetime of J-aggregates on SWNT combining lifetimes of J-aggregate excitation, followed by energy transfer, and then SWNT excitation and emission. We have obtained the lifetimes for such hybrid systems in the range of 60-105 ps (Figure 5a), being slower than the lifetimes for E_{11} PL of pristine SWNTs studied previously and ranging 5-40 ps.[31,32] The lifetimes of the free aggregates are obtained from visible range TRPL decays at λ_{EM} = 630-650 nm and the excitation of the aggregates according to Figure 2b. The free aggregate lifetimes are in the range of 400-500 ps (Figure 5b). Besides, the lifetimes of BIC monomers can be evaluated from TRPL decays in visible range for the diluted solutions of the dye. The lifetimes of BIC monomer in water equal to 330-350 ps (Figure 5b) and characterize fast cis-trans isomerization of BIC molecules in a non-rigid environment, and thus the aqueous monomer lifetime is not a lifetime of an excited molecular state in absence of nonradiative processes, τ_0.[23] We have measured the TRPL decays for BIC monomers in glycerol, where cis-trans isomerization is obstructed, obtaining τ_0 = 2.63 ns (Figure 5c).

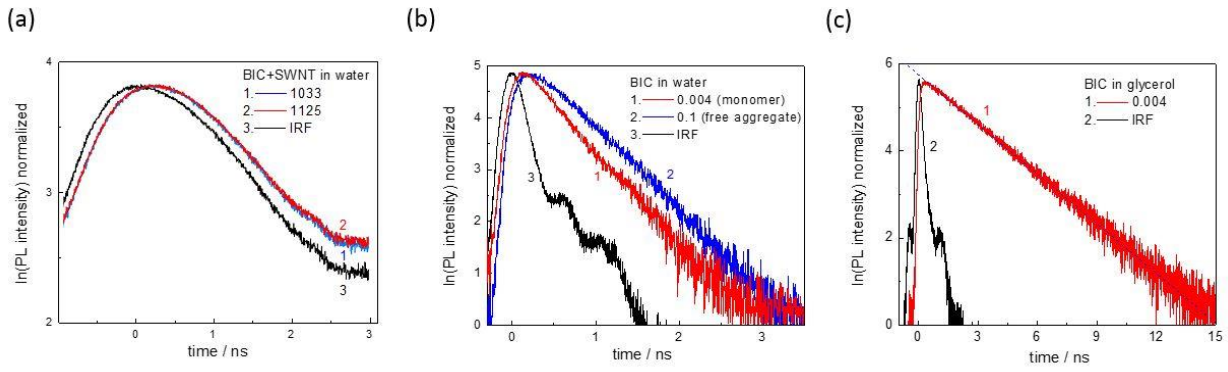

Figure 5. (a) Time-resolved PL decays (λ_{EX} = 630 nm) for the mixtures of BIC (0.004 g/L) with SWNT at λ_{EM} = 1033 nm (curve 1) and λ_{EM} = 1125 nm (curve 2); SWNT and SDBS concentrations are 0.012 and 0.13 g/L, respectively. (b) Time-resolved PL decays (λ_{EX} = 405 nm) for aqueous solutions of BIC at the concentrations of 0.004 g/L (curve 1; λ_{EM} = 610 nm) and 0.1 g/L (curve 2; λ_{EM} = 640 nm). (c) Time-resolved PL decays (λ_{EX} = 405 nm) for glycerol solutions of BIC at the concentration of 0.004 g/L (curve 1; λ_{EM} = 603 nm). Instrument Response Functions (IRF) (a,b - curves 3; c – curve 2).

Furthermore, the lifetimes allow us to characterize dynamic processes in the studied materials and to evaluate one of the most important parameters of excitonic systems, the delocalization length (N_C) of excitons in J-aggregates.[6] N_C is approximately equal to the number of molecules in the J-aggregate, if there is an ideal order or weak disorder of the molecules in the J-aggregate. In fact, N_C characterizes a resonantly conjugated length of J-aggregates or, in case of defects preventing exciton delocalization, the number of molecules in J-aggregates enabling coherent movement of the excitons. For large N_C, the narrow spectral bands and short lifetimes of the aggregates are expected. This way we can estimate the range of N_C for the J-aggregates using the formula (1)[6]

$$N_C = \frac{\pi^2}{8} \frac{\tau_{mon}}{\tau_j} \quad (1)$$

where τ_{mon} and τ_j are characteristic lifetimes of the monomers and J-aggregates, respectively. τ_{mon} = 2.36 ns, and τ_j = 400-500 ps resulting in N_C = 6-8 for free J-aggregates. The evaluation of N_C for BIC-SWNT aggregates using the hybrid lifetime (60-105 ps) in formula (1) provides unreasonable values due to a strong contribution of SWNT relaxation pathways. Therefore, another method of N_C calculation is preferable employing absorption bandwidths ratio for monomer and J-aggregate with formula (2)

$$N_C = \frac{3}{2}\left(\frac{\Delta\nu_M^{HWHM}}{\Delta\nu_J^{HWHM}}\right)^2 - 1 \quad (2)$$

where $\Delta\nu_M^{HWHM}$ and $\Delta\nu_J^{HWHM}$ are half-widths on half-maximum of the monomer and J-aggregate absorption bands in wavenumbers.[25] These can be determined from the experimental data in Figures 1d and 2a: $\Delta\nu_M^{HWHM}$ = 340 cm^{-1}, $\Delta\nu_{J-SWNT}^{HWHM} = \Delta\nu_{J-FREE}^{HWHM}$ = 90 cm^{-1}. This way, $N_C = 20 \pm 3$ for the BIC aggregates on SWNTs and free aggregates. The difference between the obtained values of N_C using lifetimes in formula (1) and half-widths in formula (2) can be attributed to the various nature of disorder contributing to N_C. Spectral shape of the J-band absorption is strongly influenced by the static disorder reflecting topological and energy disorder in J-aggregates, whereas the dynamic disorder appearing via exciton-phonon interaction has predominant effect on J-aggregate excitation lifetimes.[25] Absorption spectra of a J-band describe the Frank-Condon optical transitions in J-aggregates disregarding following relaxation of the excitation to lower energy states. Thus, N_C obtained from the formula (1) is strongly affected by the exciton dynamics in excited state and can be much lower than static N_C evaluated by the formula (2).

$N_C = 20 \pm 3$ for the free aggregates of BIC dye characterizes the condition of saturated concentration of the dye molecules enabling efficient stacking into long aggregates (Figure S2). Essentially, $\Delta\nu_{J-SWNT}^{HWHM}$ practically does not change in the studied range of SWNTs and BIC concentrations, and thus obtained $N_C = 20 \pm 3$ is a saturated value for the formed aggregates on the nanotubes leading to the maximum length of J-aggregates in the present system. Therefore, SWNT, as a scaffolding element, supports the formation of long J-aggregates with $N_C = 20 \pm 3$ at relatively low BIC concentrations.

Importantly, the narrow resonant peaks and fast relaxation lifetimes for studied conjugates of J-aggregate with SWNT in comparison with the radiative lifetime of BIC monomers evidence extensive delocalization length for J-aggregate excitons. It has to be underlined that the exciton delocalization for J-aggregates coupled to the SWNT is not limited to the obtained values of N_C, and has to be extended with a delocalization area of excitons in the nanotube via RET channel. The exciton delocalization in SWNTs is defined by the intrinsic diffusion length of excitons, which is equal to 200 nm in pristine SWNTs.[33] Such extensive delocalization area is of utmost importance for excitonic nanoscale devices, where space limitation for exciton migration without annihilation is a challenge. Considering the approximate length of BIC molecule in cis-form is 1.6 nm and the intermolecular distance of 0.7 nm in BIC J-aggregates,[29] the delocalization length of excitons in J-aggregates is 15 ± 3 nm. The integration of long J-aggregates with SWNTs is a step closer to coherently coupled nanosize devices, where J-aggregates can be positioned not only as an interface element between photonic, plasmonic and excitonic circuits,[4] but become an active element of nanoscale photonic and optoelectronic devices. Finally, the miniaturization tendency in nowadays nanoelectronics, with SWNTs in the center of such developments,[2] put forward an ultimate challenge to replace the silicon based technology with SWNT elements, able to run faster and

consume less power due to quasiballistic transport of charge carriers. Therefore, an integration of nano-size J-aggregates of ultra-high photosensitivity with SWNTs could translate the excellence in recent nanoelectronic achievements into new opportunities for nanophotonics, optoelectronics and bio-medical imaging.

Conclusions

To sum up, we have revealed for the first time a unique formation of resonant J-aggregates on the outer surface of SWNTs with efficient energy transfer from the dye aggregate to the nanotube. The proposed mechanism of the aggregate formation is associated with favorable self-assembly of cis-isomers of the BIC dye having bended π-conjugation moiety and aligning well to the convex nanotube surface. Besides to formation of J-aggregates on SWNTs, free aggregates of BIC (without SWNTs) are obtained having different spectral features and being related to self-assembly of predominantly planar trans-isomers of the BIC dye. Our findings show formation of a unique nanomaterial with advanced functionality, which paves the way towards broad chemical exploration and physical applications of efficient resonant interaction of self-assembly J-aggregates and the nanotubes in hyperspectral bio-medical imaging and treatment, nanoscale optoelectronic and photonic devices for logic, high-speed communications, and next-generation semiconductor electronic and excitonic technologies.

Supporting Information Description: supplementary absorption and PL spectra (Figure S1) TEM images and analysis (Figure S2-S4), concentration-dependent studies of the J-aggregate formation by spectral analysis (Figure S5-S7, Table S1).

Acknowledgements

P.L. and A.R. acknowledge support of Royal Academy of Engineering / The Leverhulme Trust (Senior Research Fellowship, #LTSRF1617/13/57), EU FP 'Horizon-2020' Marie Skłodowska-Curie Individual Fellowship (FOC4SIP, #654733) and RISE (CARTHER, #690945). G.E.A. and A.A.M. gratefully acknowledge the support of the Jacob Blaustein Center for Scientific Cooperation via their respective postdoctoral research fellowships. A. Upcher is acknowledged for technical assistance in acquiring high resolution TEM images.

References

(1) Cerofolini, G. *Nanoscale Devices: Fabrication, Functionalization, and Accessibility from the Macroscopic World*; Springer: Berlin Heidelberg, 2009.

(2) Kong, E. S. W. *Nanomaterials, Polymers and Devices: Materials Functionalization and Device Fabrication*; John Wiley & Sons: Hoboken, New Jersey, 2015.

(3) Whitesides, G. M.; Grzybowski, B. Self-Assembly at All Scales. *Science* **2002**, *295*, 2418-2421.

(4) Saikin, S. K.; Eisfeld, A.; Valleau, S.; Aspuru-Guzik, A. Photonics Meets Excitonics: Natural and Artificial Molecular Aggregates. *Nanophotonics* **2013**, *2*, 21-38.

(5) Würthner, F.; Kaiser, T. E.; Saha-Möller, Ch. R. J-Aggregates: From Serendipitous Discovery to Supramolecular Engineering of Functional Dye Materials. *Angew. Chem. Int. Ed*. **2011**, *50*, 3376-3410.

(6) Kobayashi, T. *J-aggregates. Volume 2*; World Scientific: Singapore, 2012.

(7) Liu, J.; Zhang, H.; Dong, H.; Meng, L.; Jiang, L.; Jiang, L.; Wang, Y.; Yu, J.; Sun, Y.; Hu, W. et al. High Mobility Emissive Organic Semiconductor. *Nat. Commun*. **2015**, *6*, 10032.

(8) Tischler, J. R.; Scott Bradley, M.; Zhang, Q.; Atay, T.; Nurmikko, A.; Bulovic´, V. Solid State Cavity QED: Strong Coupling in Organic Thin Films. *Org. Electron.* **2007**, *8*, 94-113.

(9) Beane, G.; Brown, B. S.; Johns, P.; Devkota, T.; Hartland, G. V. Strong Exciton-Plasmon Coupling in Silver Nanowire Nanocavities, *J. Phys. Chem. Lett*., **2018**, *9*, 1676-1681.

(10) Salomon, A.; Genet, C.; Ebbesen, T. W. Molecule–Light Complex: Dynamics of Hybrid Molecule–Surface Plasmon States. *Angew. Chem. Int. Ed.* **2009**, *48*, 8748-8751.

(11) Kim, K. H.; Bae, S. Y.; Kim, Y. S.; Hur, J. A.; Hoang, M. H.; Lee, T. W.; Cho, M. J.; Kim, Y.; Kim, M.; Jin, J.-I., et al. Highly Photosensitive J-Aggregated Single-Crystalline Organic Transistors. *Adv. Mater.* **2011**, *23*, 3095-3099.

(12) Shakiba, M.; Ng, K. K.; Huynh, E.; Chan, H.; Charron, D. M.; Chen, J.; Muhanna, N.; Foster, F. S.; Wilson, B. C.; Zheng, G. Stable J-aggregation Enabled Dual Photoacoustic and Fluorescence Nanoparticles for Intraoperative Cancer Imaging. *Nanoscale* **2016**, *8*, 12618-12625.

(13) Song, X.; Gong, H.; Liu, T.; Cheng, L.; Wang, C.; Sun, X.; Liang, C.; Liu, Z. J-Aggregates of Organic Dye Molecules Complexed with Iron Oxide Nanoparticles for Imaging-Guided Photothermal Therapy Under 915-nm Light. *Small* **2014**, *10*, 4362-4370.

(14) Vasa, P.; Wang, W.; Pomraenke, R.; Lammers, M.; Maiuri, M.; Manzoni, C.; Cerullo, G.; Lienau, C. Real-Time Observation of Ultrafast Rabi Oscillations Between Excitons and Plasmons in Metal Nanostructures with J-aggregates, *Nat. Photonics* **2013**, *7*, 128-132.

(15) Banal, J. L.; Kondo, T.; Veneziano, R.; Bathe, M.; Schlau-Cohen, G. S. Photophysics of J-Aggregate-Mediated Energy Transfer on DNA, *J. Phys. Chem. Lett*., **2017**, *8*, 5827-5833.

(16) Lutsyk, P.; Arif, R.; Hruby, J.; Bukivskyi, A.; Vinijchuk, O.; Shandura, M.; Yakubovskyi, V.; Kovtun, Yu.; Rance, G. A.; Fay, M.; et al. A Sensing Mechanism for the Detection of Carbon Nanotubes Using Selective Photoluminescent Probes Based on Ionic Complexes with Organic Dyes. *Light Sci. Appl.* **2016**, *5*, e16028.

(17) Lutsyk, P.; Piryatinski, Yu.; AlAraimi, M.; Arif, R.; Shandura, M.; Kachkovsky, O.; Verbitsky, A.; Rozhin, A. Emergence of Additional Visible Range Photoluminescence Due to Aggregation of Cyanine Dye - Astraphloxin on Carbon Nanotubes Dispersed with Anionic Surfactant. *J. Phys. Chem. C* **2016**, *120*, 20378-20386.

(18) Al Araimi, M.; Lutsyk, P.; Verbitsky, A.; Piryatinski, Yu.; Shandura, M.; Rozhin, A. A Dioxaborine Cyanine Dye as a Photoluminescence Probe for Sensing Carbon Nanotubes. *Beilstein J. Nanotechnol.* **2016**, *7*, 1991-1999.

(19) Gaufrès, E.; Tang, N. Y.-W.; Lapointe, F.; Cabana, J.; Nadon, M.-A.; Cottenye, N.; Raymond, F.; Szkopek, T.; Martel, R. Giant Raman Scattering from J-Aggregated Dyes Inside Carbon Nanotubes for Multispectral Imaging, *Nat. Photonics* **2014**, *8*, 72-78.

(20) Alander, J. T.; Kaartinen, I.; Laakso, A.; Pätilä, T.; Spillmann, T.; Tuchin, V.V.; Venermo, M.; Välisuo, P. A Review of Indocyanine Green Fluorescent Imaging in Surgery. *Int. J. Biomed. Imaging* **2012**, *2012*, 940585.

(21) Weiss, E.; Groenen-Serrano, K.; Savall, A. Electrochemical Mineralization of Sodium Dodecylbenzenesulfonate at Boron Doped Diamond Anodes. *J. Appl. Electrochem*. **2007**, *37*, 1337-1344.

(22) Roquelet, C.; Langlois, B.; Vialla, F.; Garrot, D.; Lauret, J. S.; Voisin, C. Light Harvesting with non Covalent Carbon Nanotube/Porphyrin Compounds. *Chem. Phys.* **2013**, *413*, 45-54.

(23) Lakowicz, J. R. *Topics in Fluorescence Spectroscopy. Principles. Volume 2*. Springer: US, 2002.

(24) Yanagi, K.; Iakoubovskii, K.; Matsui, H.; Matsuzaki, H.; Okamoto, H.; Miyata, Y.; Maniwa, Y.; Kazaoui, S.; Minami, N.; Kataura, H. Photosensitive Function of Encapsulated Dye in Carbon Nanotubes. *J. Am. Chem. Soc.* **2007**, *129*, 4992-4997.

(25) Agranovich, V. M.; Bassani, G. F. *Thin Films and Nanostructures: Electronic Excitations in Organic Based Nanostructures. Volume 31*. Elsevier Academic Press: Amsterdam, The Netherlands, 2003.

(26) Dexter, D. L. A Theory of Sensitized Luminescence in Solids. *J. Chem. Phys.* **1953**, *21*, 836-850.

(27) Heller, D. A.; Jin, H.; Martinez, B. M.; Patel, D.; Miller, B. M.; Yeung, T.-K.; Jena, P. V.; Höbartner, C.; Ha, T.; Silverman, S. K., et al. Multimodal Optical Sensing and Analyte Specificity Using Single-Walled Carbon Nanotubes, *Nat. Nanotechnol.* **2009**, *4*, 114-120.

(28) Verma, S.; Ghosh, H. N. Exciton Energy and Charge Transfer in Porphyrin Aggregate/Semiconductor (TiO2) Composites, *J. Phys. Chem. Lett*., **2012**, *3*, 1877-1884.

(29) Busse, G.; Frederichs, B.; Petrov, N. Kh.; Techert, S. Structure Determination of Thiacyanine Dye J-Aggregates in Thin Films: Comparison between Spectroscopy and Wide Angle X-Ray Scattering. *Phys. Chem. Chem. Phys.* **2004**, 6, 3309-3314.

(30) Shapiro, B. I.; Belonozhkina, E. A.; Kuz'min, V. A. Cis-, Trans-Aggregates of Thiatrimethine Cyanine Dyes. *Nanotechnol. Russ.* **2009**, *4*, 38-44.

(31) Wang, F.; Dukovic, G.; Brus, L.E.; Heinz, T. F. Time-Resolved Fluorescence of Carbon Nanotubes and Its Implication for Radiative Lifetimes. *Phys. Rev. Lett.* **2004**, *92*, 177401.

(32) Gokus, T.; Hartschuh, A.; Harutyunyan, H.; Allegrini, M.; Hennrich, F.; Kappes, M.; Green, A. A.; Hersam, M. C.; Araújo, P. T.; Jorio, A. Exciton Decay Dynamics in Individual Carbon Nanotubes at Room Temperature. *Appl. Phys. Lett.* **2008**, *92*, 153116.

(33) Xie, J.; Inaba, T.; Sugiyama, R.; Homma, Y. Intrinsic Diffusion Length of Excitons in Long Single-Walled Carbon Nanotubes from Photoluminescence Spectra. *Phys. Rev. B* **2012**, *85*, 085434.

TOC Graphic

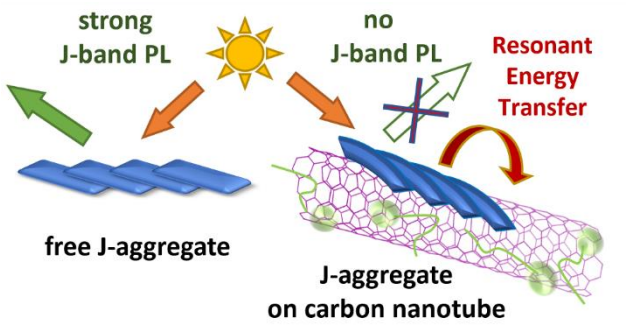
strong
J-band PL
no
J-band PL
Resonant
Energy
Transfer
free J-aggregate
J-aggregate
on carbon nanotube